Structural, dynamic, and electronic properties of liquid tin: An ab initio molecular dynamics study

L. Calderín, D. J. González, L. E. González, and J. M. López

Citation: J. Chem. Phys. **129**, 194506 (2008); doi: 10.1063/1.3020304
View online: http://dx.doi.org/10.1063/1.3020304
View Table of Contents: http://jcp.aip.org/resource/1/JCPSA6/v129/i19
Published by the American Institute of Physics.

Structural, dynamic, and electronic properties of liquid tin: An *ab initio* molecular dynamics study

L. Calderín, D. J. González, L. E. González,[a] and J. M. López
Departamento de Física Teórica, Facultad de Ciencias, Universidad de Valladolid, 47011 Valladolid, Spain

(Received 17 April 2008; accepted 17 October 2008; published online 18 November 2008)

We report on a study of several structural, dynamic, and electronic properties of liquid Sn at a thermodynamic state close to the triple point (573 K) and another one at a higher temperature (1273 K). This study has been performed by *ab initio* molecular dynamics simulations using 205 atoms and around 20 ps of simulation time. The calculated static structures show a good agreement with the available experimental data. The dynamic structure factors fairly agree with their experimental counterparts obtained by inelastic x-ray scattering experiments, which display inelastic side peaks. The calculated dispersion relations exhibit a positive dispersion, although not so marked as suggested by the experiment; moreover, its slope at the long-wavelength limit compares favorably with the experimental sound velocity. Electron densities near selected triplets of atoms are similar to those appearing in the solid phases, but these features have an extremely short lifetime, so they should not be considered as solid remnants in the melt. © *2008 American Institute of Physics*. [DOI: 10.1063/1.3020304]

I. INTRODUCTION

Molecular dynamics (MD) simulations have become an essential technique in the study of a wide variety of condensed matter systems. Classical molecular dynamics (CMD) techniques are easy to apply as the forces acting upon the ions are derived from interatomic potentials in which the electronic degrees of freedom are hidden. On the other hand, *ab initio* molecular dynamics (AIMD) methods are computationally more demanding because the forces are derived from electronic structure calculations which are performed as the MD trajectory is generated. During the last two decades, there has been a relentless increase in the development and application of AIMD methods based on density functional theory (DFT).[1,2] Given a collection of atoms with specified positions, DFT allows to determine their ground state electronic energy as well as the forces on them, via the Hellmann–Feynman (HF) theorem and Pulay corrections if necessary. Therefore, it is possible to perform MD simulations in which the ionic positions evolve according to classical mechanics while the electronic subsystem follows adiabatically.

Solid Sn is peculiar as compared to other IV B elements. At room pressure, Si, Ge, and Pb do not show any polymorphism. Si and Ge crystallize into semiconducting diamond structures, while Pb crystallizes into a metallic fcc phase. But Sn solidifies into a metallic high temperature tetragonal phase (β-Sn), and transforms into a semiconducting diamond phase (α-Sn) at lower temperatures. In the β-Sn structure each atom has four nearest neighbors, as in the diamond phase, but the six tetrahedral angles of around 109° of the diamond structure are strongly distorted in the β phase, with four angles close to 94° and two angles near 150°.

The IV B elements in the liquid state near the triple point also display a peculiar trend in their structural properties. Liquid Si and Ge retain some covalent bonding character, which is reflected in a distinctive shoulder at the high-q side of the main peak in the static structure factor $S(q)$, along with small coordination numbers (CN), around 6–7, suggesting open local structures. Conversely, l-Pb has a $S(q)$ and CN which are typical of a simple liquid metal and therefore are well described by the simple hard-sphere (HS) model. However, l-Sn shows intermediate features, with a $S(q)$ displaying a small hump at the high-q side of the main peak and a CN around 9–10.

The study of the structure of the liquid IV B elements through AIMD methods was started shortly after the appearance of this type of methods[3] by Stich *et al.*[4] who studied the static structure and also a restricted set of van Hove correlation functions for liquid Si near the melting point. The static structure of liquid Ge followed four years later by Kresse and Hafner,[5] while liquid Sn and Pb had to wait until 2002 to be studied by Kresse.[6] The *ab initio* study of their dynamic structure factor has, however, become possible only more recently, through the advent of more computer power and/or simplifying methods, as the orbital-free AIMD.[7] Studies have been performed for liquid Si,[8] Ge,[9,10] and Pb.[11]

Liquid Sn has attracted an important amount of experimental and theoretical work. Measurements have been performed for several thermodynamic magnitudes,[12–15] as well as for the static[16–20] and dynamic structure factors.[21,22] On the theoretical side a number of studies, using either semiempirical[23] or more fundamental[6,24] approaches have addressed a variety of structural and thermodynamical magnitudes. However, to our knowledge, this paper reports the first *ab initio* study on the dynamic structure of l-Sn.

On the experimental side, the $S(q)$ of l-Sn has been determined, at several temperatures within the range of

[a]Electronic mail: luisen@liq1.fam.cie.uva.es.

505–1873 K, by means of x-ray[16] (XR) and neutron[17–19] (NS) scattering experiments. Within that temperature range, the measured $S(q)$'s showed an asymmetrical main peak at $q_p \approx 2.2$ Å^{-1} along with a hump at $q \approx 2.8$ Å^{-1}. With increasing temperature, the main peak becomes lower and broader although its shape remains asymmetrical even at $T=1873$ K. As for the aforementioned hump, it progressively fades away with increasing temperature although it is still clearly visible at $T=1373$ K.

Di Cicco *et al.*[25] have also studied the short-range structure in crystalline β-Sn and *l*-Sn by means of x-ray absorption spectroscopy. The analysis of their results by using reverse Monte Carlo (RMC) techniques suggested that *l*-Sn is a mixture of low-coordinated (tetrahedral-like) configurations and high-coordinated (CN$\approx$9) structures. Indeed, previous RMC studies[26] had already hinted the possibility of some tetrahedral bonding. Similar conclusions have also been reached by Itami *et al.*[19] who also pointed the existence of tetrahedral bonding up to high temperatures.

Recently, the pressure dependence of the static structure of *l*-Sn has been investigated up to 19.4 GPa, by XR diffraction.[20] Upon compression up to 6 GPa, the structural features reflecting the anisotropic local structure become less marked (i.e., the hump at $q \approx 2.8$ Å^{-1}) indicating that the structure of *l*-Sn evolves towards that of a simple liquid. However, for higher pressures it is observed that this evolution does not occur monotonically but takes a relatively stable intermediate form with an anisotropic local structure before approaching that of a simple liquid metal.

The dynamic structure factor, $S(q,\omega)$, has been measured at $T=593$ and 1273 K by inelastic XR scattering (IXS).[21,22] Those measurements revealed the existence of collective modes lasting up to $q \approx 0.75 q_p$, as well as a positive dispersion in the low-q region, with a mode velocity at 593 and 1273 K that is about 12% and 6% greater than the respective hydrodynamic sound velocity.

Among the semiempirical works, we highlight Ref. 23 which basically resorted to the HS model in order to calculate different properties. CMD simulations were also performed by Jank and Hafner[24] for *l*-Sn near melting. They used an interatomic potential derived from a nonlocal pseudopotential with relativistic core functions. Their CMD results for the static structure showed some discrepancies with experiment, namely, the main peak of the $S(q)$ was higher than experiment, it showed no hump at $q \approx 2.8$ Å^{-1} and the subsequent oscillations were out of phase. The results for the electronic density of states suggested a metallic behavior although it clearly departed the typical free-electron parabola, with a noticeable minimum at $\approx$–4.0 eV.

The first AIMD calculation of the static structure of *l*-Sn was carried out by Kresse,[6] for a thermodynamic state near the triple point. The calculation used 96 particles, an ultrasoft Vanderbilt pseudopotential and the generalized gradient approximation for the electronic exchange and correlation energies. However, the obtained $S(q)$ exhibited some deficiencies such as a too pronounced main peak which also was slightly shifted to greater q-values along with an overestimation for the depth of the minimum. The attendant $g(r)$ showed similar problems and its oscillations were out of phase. It was claimed that the small system size was mainly responsable for these discrepancies.

Also Itami *et al.*[19] have performed AIMD calculations for the static structure of *l*-Sn for some thermodynamic states within the range 773–1873 K. They used 64 particles, the norm-conserving Troullier–Martins pseudopotential and the local density approximation for the electronic exchange and correlation energies. The calculated $S(q)$ showed good agreement with experiment although the corresponding diffusion coefficients, partly because of the small number of particles used, were somewhat smaller than experiment. Their analysis of the bond angle distributions and the CN's lead them to conclude the existence of tetrahedral bonding up to high temperatures.

In this paper we extend the AIMD study to the temperature of 573 K, which, despite being closer to the triple point, was not studied by Itami *et al.*[19] Additionally we also consider a higher temperature, 1273 K, for which experimental data for the dynamic properties are available.

The layout of the paper is as follows. In Sec. II we briefly describe the theory used in the present AIMD simulations, giving some technical details, as well as the pseudopotential describing the electron-ion interaction. In Sec. III we present and discuss the obtained structural, dynamical and electronic results, which are compared with other CMD and AIMD simulations as well as with the available experimental data. Finally, some conclusions are drawn.

II. COMPUTATIONAL METHOD

Briefly, the main characteristics of the KS-AIMD method used in this work are as follows. The total energy of N ions with valence Z, enclosed in a volume Ω, and interacting with $N_e=NZ$ valence electrons is written as the sum of the total ion energy, $E_i(\{\mathbf{R}_I\})$, and the energy of the electron system $E_e([\rho],\{\mathbf{R}_I\})$ subject to the external potential created by the ions,

$$E_T(\{\mathbf{R}_I\}) = E_i(\{\mathbf{R}_I\}) + E_e([\rho],\{\mathbf{R}_I\}), \tag{1}$$

where $\rho=\rho(\mathbf{r})$ is the electron density and $\{\mathbf{R}_I\}$ are the ionic positions. According to DFT, the ground state electron density minimizes the functional

$$E_e([\rho],\{\mathbf{R}_I\}) = T_s[\rho] + E_{\text{ext}}([\rho],\{\mathbf{R}_I\}) + E_H[\rho] + E_{\text{xc}}[\rho], \tag{2}$$

where $T_s[\rho]$ is the kinetic energy of a non-interacting electron system with density $\rho(\mathbf{r})$, $E_{\text{ext}}[\rho]$ is the electron-ion interaction energy, $E_H[\rho]$ the electrostatic Hartree energy, and $E_{\text{xc}}[\rho]$ denotes the exchange-correlation energy.

The configurations are generated under the Born–Oppenheimer approximation solving the Kohn–Sham equations on a plane-wave basis set for a given configuration of ions, calculating the forces on the ions using the HF theorem, and solving the corresponding Newton's equations for constant total energy, as implemented in the QUANTUM-ESPRESSO package.[27]

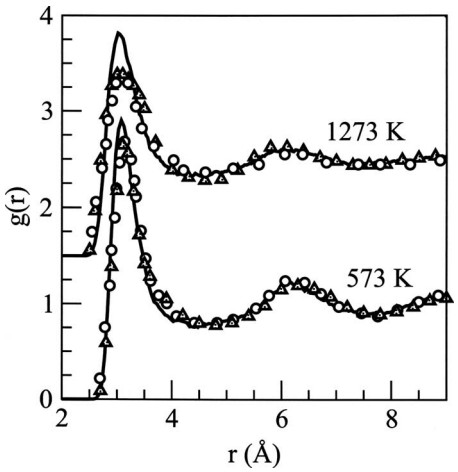

FIG. 1. Pair distribution function $g(r)$ of l-Sn at 573 and 1273 K (displaced 1.5 units). The full lines are the present AIMD results. Triangles correspond to experimental XR data at 523 and 1373 K (Ref. 16) and circles to NS data at 573 and 1373 K (Ref. 19).

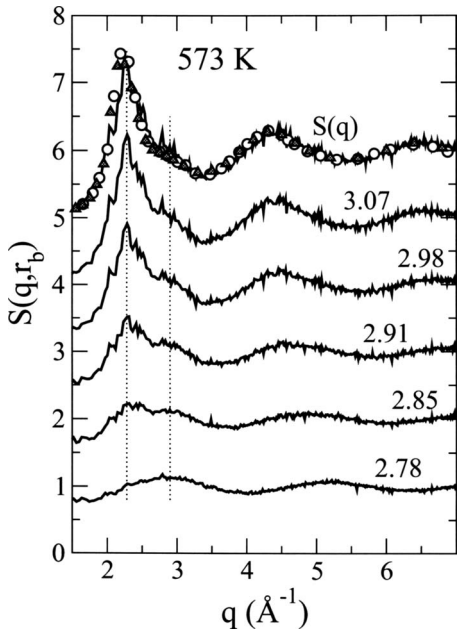

FIG. 2. "Bonded-atom" structure factors, $S(q,r_b)$ of l-Sn at 573 K. The numbers denote the value of r_b in Å. Vertical lines are drawn at the q values corresponding to main peak and the hump of $S(q)$. Triangles: experimental XR data at 523 K (Ref. 16). Circles: experimental NS data at 573 K (Ref. 19).

It is necessary to introduce an approximation for the exchange-correlation energy functional and we have adopted the local density approximation (LDA), as parametrized by Perdew and Zunger.[28]

The ion-electron interaction has been described by a norm-conserving scalar-relativistic Troullier–Martins pseudopotential[29] which was generated[27] from the atomic electron configuration $[\mathrm{Kr}](4d^{10})5s^2\ 5p^2\ 5d^0$, pseudizing the all-electron potential to generate the local part and using cutoff radii in a.u. of $r_c(\mathrm{local})=2.5$, $r_c(s)=2.0147$, $r_c(p)=2.4917$ and $r_c(d)=3.0$.

The two thermodynamic states of l-Sn for which we have performed AIMD calculations are characterized by number densities, $\rho_i=0.035\,023$ and $0.032\,98$ Å^{-3} and temperatures $T=573$ and 1273 K, respectively. We have used 205 atoms in a cubic supercell with the initial atomic positions taken at random. The systems were thermalized during 1 ps of simulation time. Therefrom, microcanonical AIMD simulations were performed over 4000 time steps, which amounted to 20.4 ps of simulation time. We have used a plane-wave representation with an energy cutoff of 12 Ryd and the single Γ point was used in sampling the Brillouin zone. We have verified that for this cutoff the total energy is converged to better than 5 mRy/atom (usually 10 mRy/atom is enough) and the forces are converged to better than 0.6 mRy/au (usually 1 mRy/au is enough). For both states, the 4000 configurations have been used in the evaluation of the respective static, dynamic, and electronic properties.

III. RESULTS AND DISCUSSION

A. Static properties

The pair distribution function, $g(r)$, provides information about the short range order in the liquid. Figure 1 depicts the obtained $g(r)$, which shows a good agreement with the corresponding experimental data. For 573 K it displays a distance of closest approach of 2.52 Å and has a main peak at 3.10 Å. This is followed by a characteristic nearly flat shape occurring between the main and the second peak. Their respective positions occur at a ratio of 2.03, larger than the value of 1.84–1.93 typical of the simple liquid metals. These structural results clearly excel a previous AIMD calculation[6] where the $g(r)$ had a main peak too high and shifted to greater r values, whereas the subsequent oscillations were somewhat out of phase. At the higher temperature of 1273 K, the present results slightly overestimate the experimental data in the first peak region, albeit its position and the subsequent oscillations are well reproduced. The maximum of $g(r)$ occurs at a somewhat smaller distance than at 573 K, around 3.02 Å, and the distance of closest approach also diminishes to 2.41 Å. This feature, also shared by liquid Ga,[30] suggests a rather soft repulsive interaction, that enables a closer approach when a higher kinetic energy is available.

To evaluate the CN we integrate the radial distribution function $4\pi r^2 g(r)$, up to the position of its first minimum, which for our calculated $g(r)$ is at $R_{\min}=3.95$ Å for both temperatures, leading to a CN of 9.4 atoms at 573 K and 8.5 atoms at 1273 K.

At 573 K, the nearest neighbor distance to a given atom is distributed within the range of 2.52–3.33 Å, with a most probable distance of 2.91 Å. As for its second, third and fourth neighbor, the most probable distances are 3.01, 3.09, and 3.17 Å, respectively; notice that these distributions overlap because of structural and thermal disorder. At 1273 K the nearest neighbor distance lies between 2.41 and 3.44 Å, with a most probable distance of 2.85 Å. The following neighbors are most probably located at the respective distances of 2.97, 3.08, and 3.19 Å.

The uppermost graph in Fig. 2 shows the calculated static structure factor, $S(q)$, at 573 K, whose main characteristics are an asymmetrical main peak located at $q_p \approx 2.26$ Å^{-1} along with a small hump at the high-q side of the

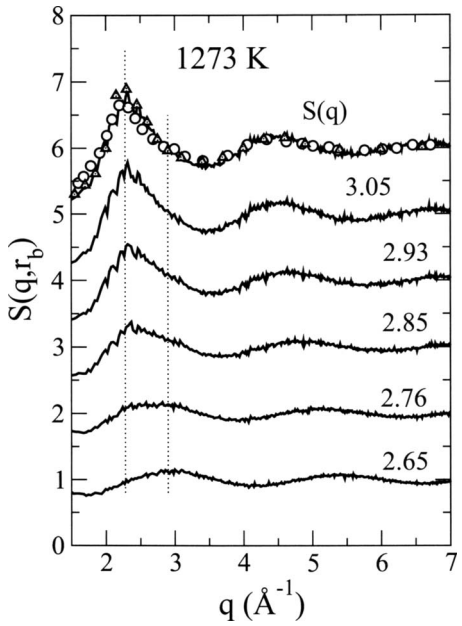

FIG. 3. The same as previous figure but for 1273 K. Experimental data are at 1373 K.

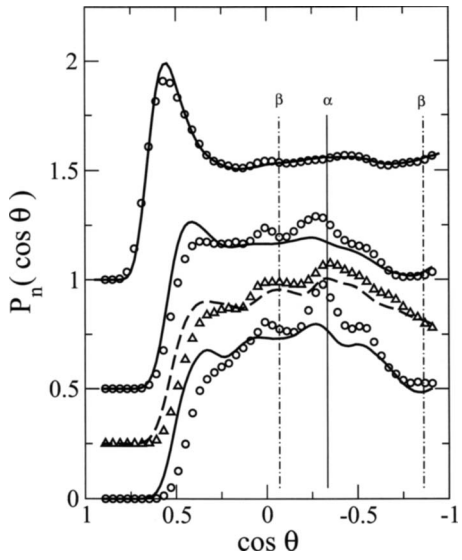

FIG. 4. Most local bond-angle distribution function, $P_2(\cos\theta)$, and the same function calculated for the first four neighbors, $P_4(\cos\theta)$ (displaced 0.5 units), and for the first nine neighbors, $P_9(\cos\theta)$ (displaced 1 unit) at $T=573$ K. Solid line: all atoms are considered. Circles: only atoms with a neighbor closer than 2.78 Å are considered as central atom in the triplet. Vertical lines denote the bond angles in the solid α and β phases. The dashed line and the triangles denote $P_2(\cos\theta)$ and its restriction, respectively, for $T=1273$ K (displaced 0.25 units).

main peak and located at 2.8 Å^{-1}. Comparison with the NS data of Itami *et al.*[19] at the same temperature and with the XR data of Waseda[16] at 523 K shows a very good agreement theory/experiment for the whole q range. Similar comments can be made on the results at the higher temperature, 1273 K, shown in Fig. 3, except that the main peak has become wider, overlaping with the hump at the higher wavevector.

The small hump in $S(q)$ reminds of the shoulder appearing in systems like *l*-Si or *l*-Ga. Based on *ab-initio* simulations for *l*-Ga, Gong *et al.*[31] were able to connect this shoulder to the existence of pairs of particles separated by very short distances; subsequently we have also confirmed that this same explanation applies to *l*-Si.[30]

In order to check if it also holds for *l*-Sn we have computed the static structure factor, $S(q,r_b)$, corresponding to only those atoms that have a neighbor closer than a distance r_b, analyzing its variations as r_b changes within the range spanned by the distribution function of the distance to the first neighbor of a given atom. Notice that for larger values of r_b, we have $S(q,r_b)=S(q)$. The results for 573 K are displayed in Fig. 2, where it is observed that the hump in $S(q)$ is at the position of the main peak corresponding to $r_b=2.78$ Å, whereas greater values of r_b lead to $S(q,r_b)$ functions with a shoulder/peak that evolves into the main peak of $S(q)$. This suggests that, as it happens in *l*-Ga and *l*-Si, the hump is induced by those pairs of atoms separated less than a cutoff distance which we take as $R_c=2.78$ Å. This value is about 8% smaller than the nearest neighbor distance in β-Sn, a magnitude rather similar to the cases of Ga and Si. Again, similar remarks can be made for $T=1273$ K, as shown in Fig. 3. Although R_c could be taken somewhat smaller than that at 573 K, we have opted by keeping the same value for ease of interpretation.

It is tempting to conjecture that the atoms involved in the appearance of the hump, i.e., those separated by distances less than R_c, display configurations remnant of those existing in the solid phases, and that the particular bonding characteristic of the solid is also partly present in the liquid. However, for a closer comparison with the solid phases, the angular distribution of the bonds between atoms is very useful. A usual way of computing the bond-angle distribution is to count any two atoms separated by less than $R_{\min}$, so that all near neighbors are included, giving rise, in our case, to an average of $9\times 8/2=36$ angles per particle for each simulation step. Sometimes smaller cutoffs are considered, at times related to certain properties of the electronic density in the liquid,[4] or by the requirement of obtaining a target average number of neighbors,[26] or taken simply as a parameter.[19,25] We consider that a more realistic picture is obtained if one includes in the computation of the bond-angle distribution only one atom and its two nearest neighbors, leading to the "most local" bond-angle distribution function, $P_2(\cos\theta)$; now one angle per particle and simulation step contributes to the distribution function. Further neighbors can orderly be included leading to increasingly delocalized functions, $P_n(\cos\theta)$, so that for n equal to the number of near neighbors, it would basically reduce to the usual bond-angle distribution. Moreover, in order to study the local structure around those atoms related to the hump in $S(q)$, $P_n(\cos\theta)$ can be computed restricting the central atom in the triplet to have a neighbor closer than R_c.

The results for $P_2(\cos\theta)$, $P_4(\cos\theta)$, $P_9(\cos\theta)$, and their restricted counterparts are shown in Fig. 4 at $T=573$ K, and for $P_2(\cos\theta)$ and its restriction at 1273 K. At 573 K we find a rich structure in the most local distribution. Apart from the typical angles for dense liquids, around 60° and 120°, further peaks appear near the tetrahedral angle and those of the β-Sn phase. These are more enhanced in the restricted calculation

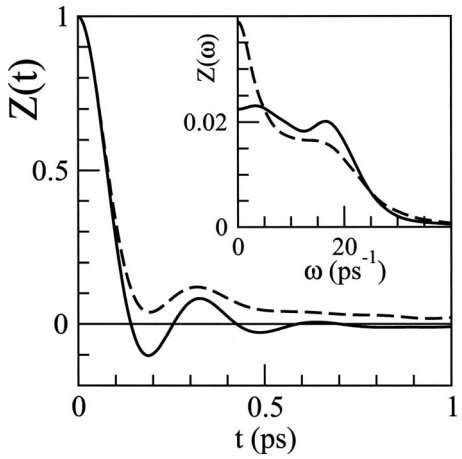

FIG. 5. Normalized velocity autocorrelation function of *l*-Sn at 573 K (full line) and 1273 K (dashed line). The inset represents its respective power spectrum $Z(\omega)$.

where only central atoms with a bond shorter than R_c are considered. This picture still remains when considering the first four neighbors of a given atom in the calculation, but it is basically washed out by disorder when the usual bond-angle distribution function (with nine neighbors) is considered. The variations brought about by increasing the temperature to 1273 K are not very pronounced, only an overall broadening of the peaks is observed but no variations in the typical angles is found.

We may conclude that *l*-Sn, even at rather high temperatures, exhibits a mixture of configurations comprising those typical of dense liquids along with others reminiscent not only of the β phase from which the solid melts, but also of the low temperature α phase. Whether the bonding in these configurations resembles that of the solid phases will be analyzed later, based on the valence electron density and the lifetime of the bonds. Let us just mention here that when one considers only atoms with a first neighbor closer than R_c, the most probable distances to the subsequent neighbors contract with respect to the unrestricted case: for $T=573$ K the second and third neighbors are most likely found at 2.94 and 3.05 Å, respectively, while at 1273 K these distances are 2.83 and 3.04 Å. This, together with the most local bond-angle distribution, has to be taken into account for the analysis of the electron density in the neighborhood of selected triplets of atoms, so that typical configurations are studied.

B. Dynamic properties

1. Single particle dynamics

For liquid systems, information about transport properties can be extracted from the velocity autocorrelation function (VACF) of a tagged ion in the fluid, $Z(t)$, which is defined as

$$Z(t) = \langle \mathbf{v}_1(t) \cdot \mathbf{v}_1(0) \rangle / \langle v_1^2 \rangle, \tag{3}$$

which stands for the normalized VACF, with $\mathbf{v}_1(t)$ being the velocity of a tagged ion in the fluid and $\langle \ldots \rangle$ standing for the ensemble average. Figure 5 depicts the calculated $Z(t)$ along with its power spectrum $Z(\omega)$ obtained by taking its Fourier transform (FT). At 573 K, $Z(t)$ exhibits the typical back-scattering behavior, with a first minimum which is not so deep as in *l*-Pb (Ref. 11) but much deeper that in *l*-Si.[8] This behavior is connected to the cage effect, and whereas the open structure (CN≈6) of *l*-Si induces a very weak back-scattering, the closed-packed structure of *l*-Pb yields a stronger backscattering and a deeper first minimum. An estimate of the frequency at which a given particle is vibrating within the cage[32] can be achieved through the short time expansion $Z(t)=1-\omega_E^2 t^2/2\ldots$, where ω_E is the so-called "Einstein frequency" of the system. A fitting of the short time region of the $Z(t)$ curve in Fig. 5 gives $\omega_E \sim 14.5$ ps^{-1} for both temperatures. The overall behavior of $Z(t)$ at 1273 K is less structured, taking always positive values, which points towards a much weaker cage effect.

The power spectrum, $Z(\omega)$, at 573 K shows two maxima located at ≈3.5 and 16.5 ps^{-1}; parenthetically we note that the covalent Sn dimer has an experimental vibrational frequency[33] of ≈5.7 ps^{-1}, which is close to the smaller maximum. At 1273 K, the high frequency peak does not change significantly in frequency, while the low frequency peak moves to $\omega=0$. Finally, we note that ω_E stands between the two peaks of $Z(\omega)$, which is a usual characteristic of simple liquid metals.[32,34]

The self-diffusion coefficient, D, can be found by either the time integral of $Z(t)$ or from the slope of the mean square displacement $\delta R^2(t) \equiv \langle |\mathbf{R}_1(t)-\mathbf{R}_1(0)|^2 \rangle$ of a tagged ion in the fluid, leading, respectively, to $D_{\mathrm{AIMD}}=0.29\pm0.02$ and 0.30 ± 0.02 Å^2/ps, at $T=573$ K. These values are close to the experimental data as measured by different techniques. Thus, Ma and Swallin[35] used the capillary method to obtain $D_{\mathrm{Exp}}=0.28\pm0.02$ Å^2/ps whereas recent experiments carried out under microgravity have yielded $D_{\mathrm{Exp}}=0.25\pm0.01$ Å^2/ps.[36]

For the higher temperature $T=1273$ K, we have obtained $D_{\mathrm{AIMD}}=1.10\pm0.04$ Å^2/ps, which also compares reasonably with the available experimental data, namely, $D_{\mathrm{Exp}}=1.14(\pm0.05)$ Å^2/ps obtained by the shear cell technique used by Bruson and Gerl[37] or the interpolated result from microgravity experiments by Itami *et al.*, $D_{\mathrm{Exp}}=1.40(\pm0.03)$ Å^2/ps.[38] At this stage is worth mentioning that the AIMD calculations of Itami *et al.*[19] yielded substantially smaller values for D, which they attributed to the smaller number of particles used in their simulations; for instance, for $T=1273$ K their estimate was $D_{\mathrm{AIMD}} \approx 0.78\pm0.04$ Å^2/ps which is around 40% smaller than experiment.

On a theoretical standpoint, mode-coupling (MC) theories, and in particular Sjogren *et al.*'s formulation,[39] have provided considerable insight into the atomic dynamics of liquids; moreover their application to simple liquids has yielded reasonable estimates for several dynamic properties.[34] Within this approach, a central magnitude is the memory function of the normalized VACF, $K(t)$ which is defined by the following equation (the dot means time derivative):

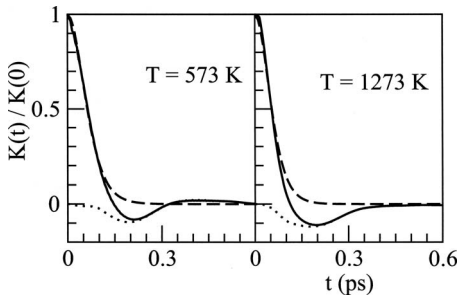

FIG. 6. Normalized memory functions $K(t)$ (full line) along with its two components, $K_B(t)$ (dashed line) and $K_{MC}(t)$ (dotted line) for the velocity autocorrelation functions of *l*-Sn at 573 and 1273 K.

$$\dot{Z}(t) = -\int_0^t dt' K(t-t')Z(t'), \tag{4}$$

and is usually split into two contributions,[34,39]

$$K(t) = K_B(t) + K_{MC}(t) \tag{5}$$

that represent two distinct dynamical regimes. $K_B(t)$ is a short time term accounting for uncorrelated binary collisions, whereas $K_{MC}(t)$, the mode-coupling term, is a long time contribution describing the effects from collective processes associated with multiple collisions. The $K_B(t)$ has usually been represented by a semiphenomenological expression, namely,

$$K_B(t) = K(0)\mathrm{sech}^2(t/\tau_B),$$
$$\tau_B = [|\ddot{K}(0)/2K(0)|]^{-1/2}. \tag{6}$$

The previous formalism combined with the interatomic pair potencial approach for the atomic interactions has been widely used in the study of the single particle dynamics of simple liquids.[34] However, recent calculations[40,41] have cast doubts about the reliability of the previous scheme in the case of some liquid metals, such as *l*-Ge, *l*-Sn, and *l*-Pb near melting. The problem hinges on the memory function $K(t)$ taking negative values before going to zero, and it is precisely those negative values which are difficult to describe by Sjogren *et al.*'s MC approach. In order to check whether this behavior of the $K(t)$ could be influenced by a pair potential description of the atomic interactions, we have used the AIMD $Z(t)$ along with Eqs. (4)–(6) to derive the associated $K(t)$, $K_B(t)$, and $K_{MC}(t)$, which are depicted in Fig. 6. For both temperatures $K(t)$ decreases with time, takes a negative value and, whereas at 573 K goes to zero with a damped oscillation, for 1273 K it approaches zero without oscillations. Consequently, the associated $K_{MC}(t)$ is always negative at the higher temperature and mostly negative for $T=573$ K. These results qualitatively agree with other earlier calculations[40,41] and therefore support the claim that Sjogren *et al.*'s MC formulation[39] fails to provide a fair description of the single particle dynamics in *l*-Sn.

Another interesting magnitude is the self-intermediate scattering function, $F_s(\mathbf{q},t)$, which describes the single-particle dynamics over different length scales, ranging from the hydrodynamic to the free-particle limit. This is defined as

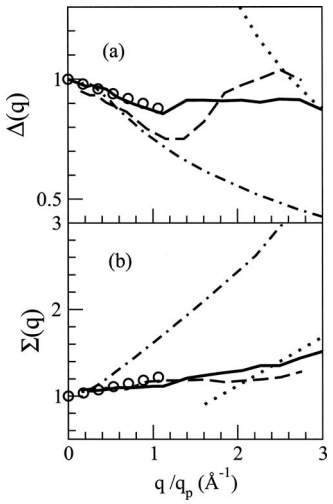

FIG. 7. (a) Normalized HWHM of $S_s(q,\omega)$, relative to its value at the hydrodynamic limit, for *l*-Sn at $T=573$ K (continuous line), *l*-Si at $T=1740$ K (dot-dashed line) and *l*-Pb at $T=650$ K (dashed line). The dotted line gives the free-particle limit for *l*-Sn. The open circles are the predictions of the mode-coupling theory for *l*-Sn. (b) Same as above, but for the normalized peak value $S_s(q,\omega=0)$, relative to its value at the hydrodynamic limit.

$$F_s(\mathbf{q},t) = \frac{1}{N}\left\langle \sum_{j=1}^{N} e^{-i\mathbf{q}\cdot\mathbf{R}_j(t+t_0)} e^{i\mathbf{q}\cdot\mathbf{R}_j(t_0)} \right\rangle. \tag{7}$$

For isotropic and homogeneous systems these correlation functions depend only on the modulus $q=|\mathbf{q}|$. Parenthetically, we note that the VACF can also be calculated as the $q\to 0$ limit of the first-order memory function of the $F_s(q,t)$. Our results for the $F_s(q,t)$ display the usual monotonic decay with time and comparison with previous AIMD results[8,11] for *l*-Si and *l*-Pb shows that, at similar (q/q_p) values, their decay is faster than in *l*-Pb but slower than in *l*-Si.

The time FT of $F_s(q,t)$ gives its frequency spectrum, $S_s(q,\omega)$, known as the self-dynamic structure factor, which has experimental relevance due to its connection with the incoherent part of the inelastic neutron scattering (INS) cross section. $S_s(q,\omega)$ exhibits, for all q values, a monotonic decay with frequency and is usually characterized by the peak value, $S_s(q,\omega=0)$, and the half-width at half-maximum (HWHM), $\omega_{1/2}(q)$. Moreover these magnitudes are frequently reported as normalized to their hydrodynamic $(q\to 0)$ limit value, by introducing the dimensionless quantities $\Sigma(q)=\pi q^2 D S_s(q,\omega=0)$ and $\Delta(q)=\omega_{1/2}(q)/q^2 D$. The present AIMD results for $\Delta(q)$ and $\Sigma(q)$ at $T=573$ K are depicted in Fig. 7 along with other AIMD results for *l*-Si[8] and *l*-Pb[11] near melting. These magnitudes exhibit a behavior which changes markedly when moving from *l*-Si to *l*-Sn and *l*-Pb, with the latter one exhibing a pattern typical of the simple liquids near melting. Indeed, it has been found that in simple liquid metals near their triple point, the $\Delta(q)$ exhibits a minimum around $q/q_p \approx 1$ which can also be related to the cage effect but for greater q values $\Delta(q)$ increases towards the binary and ultimately the free particle $(q\to\infty)$ limits. On the other hand the open structure of *l*-Si entails the virtual disappearance of the cage effect and the associated $\Delta(q)$ and $\Sigma(q)$ exhibit a behavior similar to that of a dense gas. The

case of *l*-Sn is somewhat intermediate as it experiences a weak cage effect which is reflected in the existence of a shallow minimum in the corresponding $\Delta(q)$, but as q increases it remains below its hydrodynamic value and eventually approaches the free particle limit.

Within the MC theories, the formulation of de Schepper and Ernst[42] was focused in the small-q behavior of $\Delta(q)$ and $\Sigma(q)$, and it has been found that in some simple liquids these magnitudes can be reliably described by the expressions,[43,44]

$$\Delta(q) = 1 + H(\delta)q/q^*, \quad \Sigma(q) = 1 + G(\delta^{-1})q/q^*, \tag{8}$$

where $q^* = 16\pi m\rho_i D^2/(k_B T)$, $\delta = D/(D + \eta/m\rho_i)$, with η denoting the shear viscosity, and the functions $H(\delta)$ and $G(\delta^{-1})$ are given in Ref. 43. In both equations the first term is the hydrodynamic result and the second one accounts for the coupling of mass diffusion with collective modes. The AIMD results for D (see above) and η (next section) have been used to evaluate the $\Delta(q)$ and $\Sigma(q)$ acording to Eq. (8) and the results are also depicted in Fig. 7. There is a fair agreement, similar to that found for other simple metals, which underscores the ability of the previous expresions to describe the small-q single particle dynamics in *l*-Sn near melting.

2. Collective dynamics

The collective dynamics of density fluctuations in the liquid is usually described by the intermediate scattering function, $F(q,t)$, defined as

$$F(q,t) = \frac{1}{N}\left\langle \left(\sum_{j=1}^{N} e^{-i\mathbf{q}\cdot\mathbf{R}_j(t+t_0)} \right)\left(\sum_{l=1}^{N} e^{i\mathbf{q}\cdot\mathbf{R}_l(t_0)} \right) \right\rangle, \tag{9}$$

where N is the total number of particles and $\mathbf{R}_j(t)$ is the position of the jth ion at time t.

The present AIMD simulations have lasted for ≈20 ps which implies that in the calculation of time-dependent magnitudes the number of configurations available for computing averages quickly decreases as the time increases. This is usually reflected in the appearance of some noise. For the specific case of $F(q,t)$, we have tried to overcome this difficulty by fitting the calculated $F(q,t)$'s to an analytical expression, based on a generalized hydrodynamic aproximation, which interpolates among the hydrodynamic (valid for $q \to 0$) and viscoelastic (accurate for $q \sim q_p$) models,[45] namely,

$$\frac{F(q,t)}{S(q)} = A\exp(-at) + B\exp(-bt)\cos(\omega_0 t) + C\exp(-bt)\sin(\omega_0 t). \tag{10}$$

This expression, which has six q-dependent paramenters, recovers the hydrodynamic expression of $F(q,t)$ in the small q region,[32] where the different coefficients behave as

$$A \to \frac{\gamma - 1}{\gamma}, \quad B \to \frac{1}{\gamma}, \quad C \to \frac{d}{\gamma}q, \quad a \to D_T q^2, \quad b \to \Gamma q^2, \quad \omega_0 \to c_s q, \tag{11}$$

where $\gamma = C_p/C_v$ is the ratio of specific heats, c_s is the adiabatic sound velocity, Γ the sound attenuation constant, $D_T = \kappa_T/(\rho_i C_p)$ is the thermal diffusivity, with κ_T being the thermal conductivity, and d is a coefficient that involves γ, Γ, c_s, and D_T.

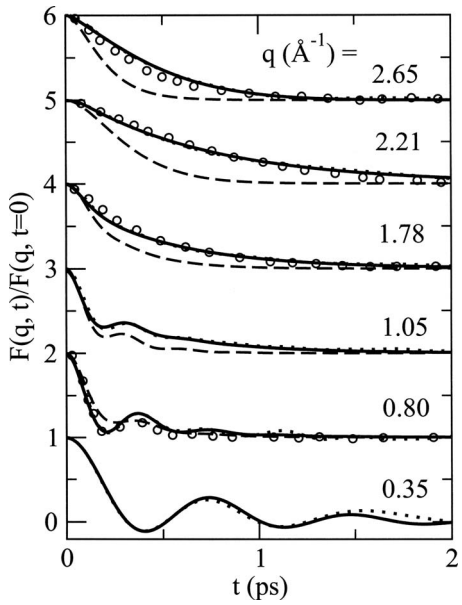

FIG. 8. Intermediate scattering function, $F(q,t)$, for several q-values. Dotted lines: present AIMD results for *l*-Sn at 573 K. Full and dashed lines: fitting of the AIMD results to the analytical expression given in Eq. (10) for $T = 573$ and 1273 K, respectively. Open circles: calculations by Hosokawa *et al.* (Ref. 21) from their experimental $S(q,\omega)$'s at $T = 593$ K and for $q = 0.81$, 1.91, 2.21, and 2.65 Å^{-1}.

Figure 8 depicts the calculated AIMD $F(q,t)$'s along with the results of the fitting scheme according to Eq. (10). Indeed, the short time behavior is unaffected by the fitting procedure and its main effect is to smooth the long time behavior of the $F(q,t)$, specially for $q \leqslant 1$ Å^{-1}.

Up to $q \approx 0.7 q_p$ Å^{-1}, the $F(q,t)$'s display an oscillatory behavior with the amplitude of the oscillations being greater for the smaller q values. This is a typical behavior of simple liquid metals near melting, as found in both computer simulations[46–49] and theoretical models.[50] However, at low q values ($q \leqslant 0.5\ q_p$) the $F(q,t)$'s already exhibit an important diffusive component which imposes a slow decay; indeed a similar trend has already observed in other group IV B liquid metals such as liquid Si, Ge, and Pb.[8,9,11] This is at variance with the results for the simple liquid metals (i.e., alkalis, alkali earths, Al) near melting,[46–50] where for a comparable q-range the diffusive component is already very weak and the corresponding $F(q,t)$'s shows marked oscillations around zero.

The time FT of the $F(q,t)$ gives the dynamic structure factor, $S(q,\omega)$, which is directly connected to the intensity scattered in an INS or IXS experiment. We can compute these functions either by direct numerical FT or as the analytical FT of the functions obtained from the fitting, leading to very similar results. This analytical FT yields a sum of a quasielastic Lorentzian peak and a pair of stretched Lorentzian inelastic peaks. In the hydrodynamic region these reduce to the two inelastic propagating peaks centered at $\omega = \pm c_s q$ with HWHM determined by Γ, and the diffusive peak at $\omega = 0$ and whose width is determined by the thermal diffusivity D_T.

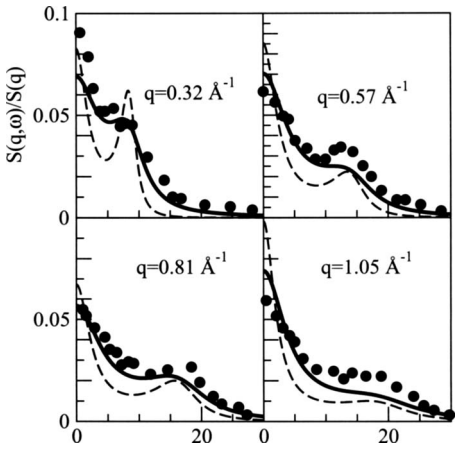

FIG. 9. Dynamic structure factor, $S(q,\omega)$, at several q values, for l-Sn at $T=573$ K. Full circles: experimental IXR data at 593 K (Refs. 21 and 22). Full and dashed lines: AIMD results for $q=0.35$, 0.60, 0.78, and 1.05 Å^{-1}, after and before convolution with the experimental resolution function, respectively.

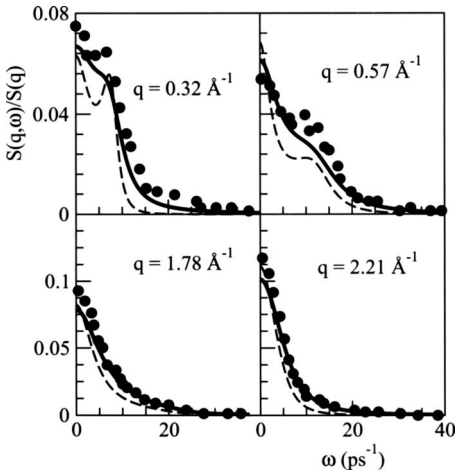

FIG. 11. Dynamic structure factor, $S(q,\omega)$, at several q values, for l-Sn at $T=1273$ K. Full circles: experimental IXR data (Refs. 21 and 22). Full and dashed lines: AIMD results for $q=0.34$, 0.59, 1.77, and 2.24 Å^{-1}, after and before convolution with the experimental resolution function, respectively.

Figures 9 and 10 show for l-Sn at 573 K a set of several $S(q,\omega)$ as functions of ω for different wavevectors up to q values slightly greater than q_p. There are well defined side peaks, indicative of collective density excitations, which last up to $q\approx(3/5)q_p$; therefrom the side peaks become shoulders up to $q\approx1.5$ Å^{-1} and for larger q values the $S(q,\omega)$ show a monotonic decreasing behavior. However, a proper comparison with the IXS data of Hosokawa *et al.*[21,22] requires the prior convolution of the previously calculated $S(q,\omega)$ with the experimental resolution function[21,22] as well as including the correction due to the detailed balance.[34] The modified $S(q,\omega)$ are also included in Figs. 9 and 10 and they show a good agreement with the experimental IXS data at $T=593$ K. Notice that the convolution with the resolution function has the effect of widening the side peaks, albeit maintaining its positions, and reducing the contact $(\omega=0)$ values. A similar comparison is provided in Fig. 11 for $T=1273$ K.

From the positions of the side peaks, $\omega_m(q)$, the dispersion relation of the density fluctuations is obtained and its slope at $q=0$ provides an estimate for the adiabatic sound velocity, c_s. Thus, for l-Sn at $T=573$ K and using the position of the side peak at the smallest q value attained by the simulation $(q_{\min}=0.349$ Å$^{-1})$, we obtain a value $c_s=2350\pm150$ m/s. Had we taken the maxima of the longitudinal current correlation function, $C_L(q,\omega)=\omega^2S(q,\omega)$, at $q_{\min}$, the estimate would be very similar, namely, $c_s=2370\pm150$ m/s. In any case, both estimates are close to the corresponding experimental data[13] of $c_s=2448$ m/s. For $T=1273$ K, we have obtained $c_s=2250\pm150$ m/s (side peaks) and $c_s=2300\pm150$ m/s (longitudinal current) which again compare well with experiment, i.e., $c_s=2284$ m/s.[21,51]

Hosokawa *et al.*[21,22] determined the q-dependent adiabatic sound velocity $c_s(q)$, by fitting the inelastic component of their measured $S(q,\omega)$ to the damped harmonic oscillator model.[52] Their $c_s(q)$ data exhibit, in the low-q region, a significant *positive dispersion*, i.e., an increase with respect to the hydrodynamic adiabatic speed of sound, with a maximum located around 0.3 Å^{-1} and whose magnitude amounts to $\approx12\pm3\%$ at 593 K. This is depicted in Fig. 12 along with our calculated $c_s(q)$ which have been obtained from the side peaks in the $S(q,\omega)$ and also from the maxima in the spectra of the longitudinal current correlation function. Notice that for $q\leqslant0.5$ Å^{-1} the estimates by Hosokawa *et al.*[21,22] are

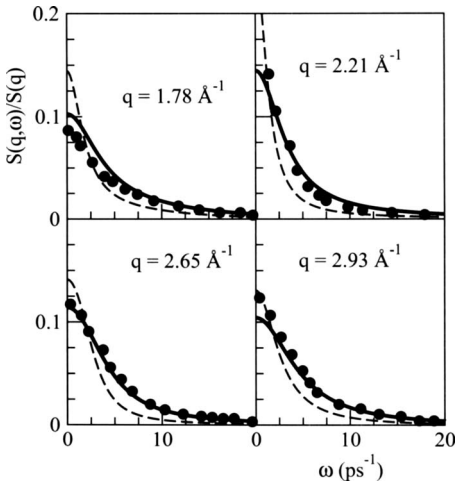

FIG. 10. Same as in Fig. 9, but for other q values.

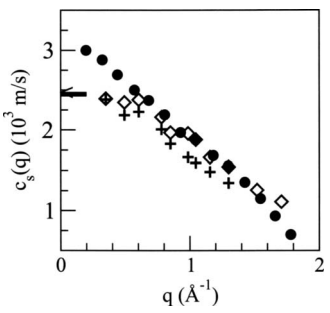

FIG. 12. q-dependent sound velocity $c_s(q)$, in l-Sn at 573 K. Full circles: Experimental data for l-Sn at 593 K (Refs. 21 and 22). Crosses: AIMD results obtained from the inelastic peaks in the $S(q,\omega)$. Open diamonds: AIMD results from the maxima in the spectra of the longitudinal current, $C_l(q,\omega)$. The arrow stands at the experimental adiabatic sound velocity.

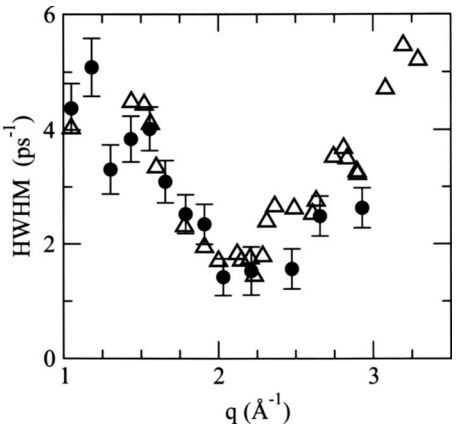

FIG. 13. HWHM of the dynamic structure factor for *l*-Sn. Full circles with error bars: Experimental data at 593 K (Refs. 21 and 22). Triangles: present AIMD results for $T=573$ K.

clearly greater than the present AIMD values. However, it should not be ruled out the possibility that Hosokawa *et al.*'s values be somewhat overblown because their calculation did not take into account the quasielastic component of $S(q,\omega)$ in the fitting. Therefore, their claim about the existence and magnitude of the *positive dispersion* is not fully substantiated. Unfortunately, the present AIMD results do not reach small enough q values so as to allow a clear analysis about the existence of a *positive dispersion*, although it seems that *if* it exists, it should take a smaller magnitude than that suggested by Hosokawa *et al.*[21,22]

For small q values, the $S(q,\omega)$ can be well described as the sum of three Lorentzians, but for greater q's the central Lorentzian curve which stands for the quasielastic extended heat mode becomes dominant. Figure 13 shows the experimental data for the HWHM of this quasielastic heat mode at $T=593$ K; it exhibits oscillations clearly connected with those of the $S(q)$. Most noticeable are the minima at $q\approx q_p$ and the shoulder at $q\approx 2.8$ Å^{-1}, with the latter being related to the hump in the $S(q)$. These features are also reproduced by the AIMD results at 573 K, which once again, show a fair agreement with experiment.

It is worth mentioning that Hosokawa *et al.*[21] used their experimental $S(q,\omega)$ to derive the attendant $F(q,t)$ functions. This was performed within a memory function formalism[34] where the second-order memory function of the $F(q,t)$ was appproximated by an expression containing two exponential decay channels for viscous relaxation and one exponential for thermal relaxation. Figure 8 depicts some of their results which show a remarkable cualitative agreement with the present calculations.

Associated with the density fluctuations is the current due to the overall motion of the particles, i.e.,

$$\mathbf{j}(q,t)=\sum_{l=1}^{N}\mathbf{v}_l(t)\exp[i\mathbf{q}\cdot\mathbf{R}_l(t)], \tag{12}$$

which is usually split into a longitudinal component, $\mathbf{j}_L(q,t)$ parallel to $\mathbf{q}$, and a transverse component, $\mathbf{j}_T(q,t)$, perpendicular to $\mathbf{q}$. Therefore, the transverse current correlation function, $C_T(q,t)$, is obtained as

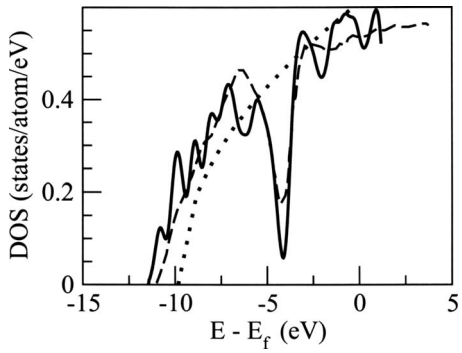

FIG. 14. Total electronic density of states for *l*-Sn. Full line: present results with eight k points. Dashed line: results by Jank and Hafner (Ref. 24). Dotted line: free electron EDOS.

$$C_T(q,t)=\langle\mathbf{j}_T(q,t)\cdot\mathbf{j}_T^*(q,0)\rangle.$$

The $C_T(q,t)$ is not directly linked to any measurable magnitude and can only be determined by means of computer simulations or some theoretical model. It gives information on the shear modes and its shape evolves from a Gaussian, in both q and t, at the free particle limit, towards a Gaussian in q and exponential in t at the hydrodynamic limit, whereas for intermediate q values, the $C_T(q,t)$ exhibits a more complicated behavior. Its spectrum, $C_T(q,\omega)$, when plotted as a function of ω, may show peaks within some q range, which are connected with propagating shear waves. The present AIMD calculations for *l*-Sn have produced $C_T(q,\omega)$'s which display peaks for a very narrow range, namely, $0.4q_p\leqslant q\leqslant 0.6q_p$. For comparison, we mention that for the simple liquid metals the equivalent range is $0.07q_p\leqslant q\leqslant 3.0q_p$, which basically coincides with the range obtained by recent AIMD calculations[11] for *l*-Pb near melting. Conversely, AIMD calculations for *l*-Si (Ref. 8) near melting have shown that the associated $C_T(q,\omega)$ show no peaks at any q value. Finally, we mention that no peaks are found in the present results for *l*-Sn at $T=1273$ K.

The shear viscosity coefficient η can be calculated from the previously obtained $C_T(q,t)$ and details about the procedure are given in Refs. 34, 46, 53, and 54. The present AIMD calculations lead to an estimate $\eta_{\mathrm{AIMD}}=1.70\pm0.08$ GPa ps and the experimental value for *l*-Sn at melting (505 K) is $\eta=1.97$ GPa ps,[55] which when extrapolated to $T=573$ K reduces to $\eta\approx 1.68$ GPa ps. Other measurements have produced comparable values such as $\eta\approx 1.56$ (Ref. 14) or 1.67 (Ref. 15) GPa ps. For $T=1273$ K, this calculation gives $\eta_{\mathrm{AIMD}}=0.90\pm0.10$ GPa ps which again compares well with the experimental data $\eta=0.90$,[55] $\eta=0.80$ GPa ps.[15]

C. Electronic properties

1. Density of states

Figure 14 shows the results obtained for the single-particle electronic density of states (EDOS), $n(E)$, which is similar for both temperatures considered. It has been obtained from the self-consistent eigenvalues, averaged over eight ionic configurations well separated in time and sampling over eight $\mathbf{k}$ points.

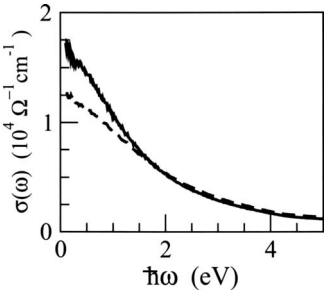

FIG. 15. Frequency dependent optical conductivity of liquid Sn as derived from the Kubo–Greenwood formula. Full and dashed lines: present results with eight **k** points for $T=573$ and 1273 K, respectively.

The bottom of the conduction band lies at −11.5 eV which is below that of the free-electron bandwidth, at −9.9 eV. The $n(E)$ is not parabolic, and it is split by a deep minimum at −4.2 eV that separates s and p dominated subbands. The previous calculations by Jank and Hafner[24] qualitatively agree with ours.

We note that when the sampling is performed using the Γ-point only, the EDOS exhibits more noise, as expected, but it also shows a deeper minimum. The noise is substantially reduced when more **k** points are included in the sampling of the Brillouin zone.

2. Electrical conductivity

We have also evaluated the electrical conductivity σ, which as in other previous *ab initio* calculations,[56] has been computed by the Kubo–Greenwood formula.[57] It is obtained by extrapolating to zero frequency, using Drude's model formula, the optical conductivity, $\sigma \equiv \sigma(0) = \lim_{\omega \to 0} \sigma(\omega)$, where $\sigma(\omega)$ is computed by a configurational average of

$$\sigma(\omega, \{R_I\}) = \frac{2\pi e^2}{3m_e^2 \Omega \omega} \sum_{i,j} (f_i - f_j) |\langle \psi_i | \hat{p} | \psi_j \rangle|^2 \times \delta(E_j - E_i - \hbar\omega), \quad (13)$$

where e and m_e are the electronic charge and mass, $\hat{p}$ is the momentum operator and ψ_i, E_i are the electronic DFT eigenstates and eigenvalues respectively for the ionic configuration $\{R_I\}$. The f_i are the Fermi–Dirac occupation numbers of the ith eigenstate. As before, we have averaged over eight ionic configurations and eight **k** points. The results obtained are shown in Fig. 15, whose relative errors would range 5%–10%. The electrical conductivity obtained is $\sigma = 0.017 \pm 0.001$ $(\mu\Omega\ \text{cm})^{-1}$ at 573 K, which is in fair agreement with the experimental value[58] $\sigma = 0.020$ $(\mu\Omega\ \text{cm})^{-1}$. For the higher temperature of 1273 K, a similar calculation yields $\sigma = 0.013 \pm 0.001$ $(\mu\Omega\ \text{cm})^{-1}$ whereas the experimental value[58] is $\sigma = 0.015$ $(\mu\Omega\ \text{cm})^{-1}$.

3. Electron density and bonding

In order to clarify the nature of the bonding between atoms involved in the hump of $S(q)$ we have plotted in Fig. 16 the valence electron pseudodensity around two typical triplets of atoms in configurations akin to the those of the solid phases. In both cases the distance between the central atom and its closest neighbor is 2.74 Å (i.e., smaller than

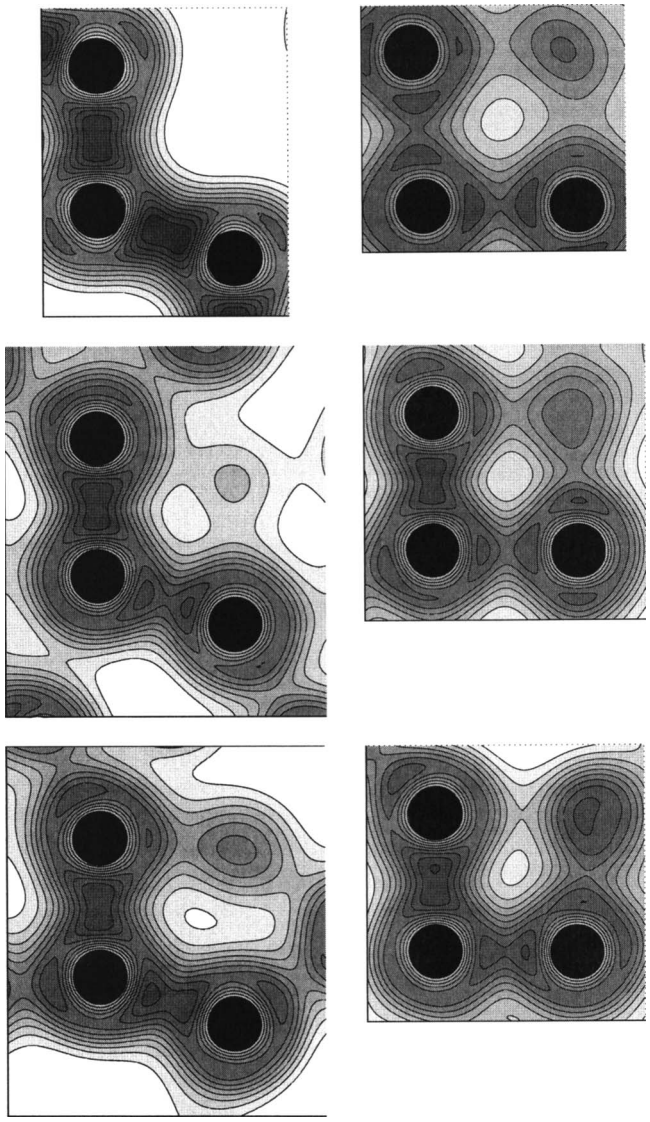

FIG. 16. Valence electron densities. First line solid structures (left: α-Sn, right: β-Sn). Second line: selected liquid configurations at 573 K. Third line: selected liquid configurations at 1273 K. The contour lines surrounding the white areas correspond to 0.01 electrons/(a.u.^{3}), and the other contour values increase in steps of 0.004. Black circles show the atomic positions.

R_c), and the distance to the second neighbor is the most problable one, i.e., 2.94 Å at 573 K and 2.83 Å at 1273 K. The angles chosen are around 109 (α-Sn-like) and 90 (β-Sn-like) degrees. Comparison is also made with the corresponding densities in the solid phases, whose interatomic distances are 2.81 and 3.02 Å for the α and β structures, respectively.

The densities in the liquid configurations shown are remarkably similar to the those of the corresponding solids, although charge accumulation between the atoms is smaller in the α-like liquid configuration than in the solid α-phase, and larger in the β-like liquid configuration than in the solid β-structure.

Although similar to the solid structures at a static level, it is also necessary to analyze the time variation of the bonding between the atoms involved in the hump of $S(q)$ in order to ascribe a physical reality to these bonds. We have calculated the distribution function of the lifetimes of the pairs

separated by less than 2.78 Å, and found a very short average lifetime of 0.041 ps at 573 K and 0.053 ps at 1273 K. Moreover, the time variation of the distance between the atoms of the pairs is collisionlike rather than transient-bonding-like.

Therefore we can conclude that the electronic density around pairs of atoms involved in the hump is akin to that in the solid phases, but the dynamic behavior of these pairs is hard to reconcile with an interpretation in terms of bonded solidlike units that exist in the melt during a reasonable, nonephemeral, transient time.

IV. CONCLUSIONS

An *ab initio* molecular dynamics simulation method has been used to calculate a whole range of static, dynamic, and electronic properties of *l*-Sn at two thermodynamic states.

The results for the static structure are in good agreement with the available experimental data. Through the most local bond-angle distibution function we have been able to qualify previous claims about the local ionic structure, which shows configurations typical of dense liquids, and also similar to the β-Sn phase, from which the system melts, and to the low temperature tetrahedral α-phase. The small hump in $S(q)$ is related to the existence of pairs of atoms of short length, whose local structure shows emphasized solidlike configurations, and whose electronic density is very similar to the corresponding solid one. However, these structures live only for an ephemeral time, even near melting, and therefore cannot be considered as real remnants of the solid phases.

The main focus of this AIMD calculation has been directed towards the study of several dynamical properties in *l*-Sn which have been recently measured[21,22] by means of IXS experiments.

The obtained VACF has a memory function that takes negative values before going to zero. This feature coincides with earlier results derived within a pair potential framework and therefore supports the claim that Sjogren's formulation of the MC theory will not properly describe the single particle dynamics in *l*-Sn.

The intermediate scattering functions, $F(q,t)$, have at low-q values an important diffusive component which although weaker than that in *l*-Si (Ref. 8) is nonetheless much stronger than in *l*-Pb or other simple liquid metals. The calculated dynamic structure factors, $S(q,\omega)$, show an overall very good agreement with their experimental counterparts. They also exhibit side peaks, indicative of collective density excitations, over a similar range of wavelengths as those in liquid simple metals.

Earlier analysis of the IXS data have suggested a positive dispersion which near melting reaches a maximum value of about 12% in the dispersion relation.[21,22] The present AIMD calculations have not reached small enough q values so as to unambiguously confirm this feature but they strongly point towards a smaller magnitude of the positive dispersion.

The transverse current correlation functions, $C_t(q,t)$, have a spectra, $C_t(q,\omega)$, which near melting shows inelastic peaks only within a very narrow q range, while they disappear completely at the higher temperature. In this respect, *l*-Sn shows an intermediate behavior between *l*-Si (no inelastic peaks at all) and *l*-Pb (inelastic peaks over a wide range). These results further support the link, suggested in a previous AIMD study[8] on *l*-Si, between the existence of inelastic peaks in the $C_t(q,\omega)$ and the magnitude of CN and its influence on the strength of the cage effect.

The calculated transport coefficients, both atomic, such as the adiabatic sound velocity, self-diffusion and shear viscosity coefficients, and electronic, like the electrical conductivity, have shown a very good agreement with experiment at the two temperatures considered.

ACKNOWLEDGMENTS

L.C. acknowledges the financial support of the Ministerio de Educacion y Ciencia of Spain (SB2005-0062). D.J.G., L.E.G., and J.M.L., acknowledge the support of the DGICYT (MAT2005-03415), the EU FEDER program, and Junta de Castilla y León (VA068A06).

[1] P. Hohenberg and W. Kohn, Phys. Rev. **136**, B864 (1964).
[2] W. Kohn and L. J. Sham, Phys. Rev. **140**, A1133 (1965).
[3] R. Carr and M. Parrinello, Phys. Rev. Lett. **55**, 2471 (1985).
[4] I. Stich, R. Car, and M. Parrinello, Phys. Rev. Lett. **63**, 2240 (1989); Phys. Rev. B **44**, 4262 (1991); I. Stich, Phys. Rev. A **44**, 1401 (1991); I. Stich, M. Parrinello, and J. M. Holender, Phys. Rev. Lett. **76**, 2077 (1996).
[5] G. Kresse and J. Hafner, Phys. Rev. B **47**, 558 (1993).
[6] G. Kresse, J. Non-Cryst. Solids **312–314**, 52 (2002).
[7] M. Pearson, E. Smargiassi, and P. A. Madden, J. Phys.: Condens. Matter **5**, 3221 (1993).
[8] A. Delisle, D. J. González, and M. J. Stott, Phys. Rev. B **73**, 064202 (2006); J. Phys.: Condens. Matter **18**, 3591 (2006).
[9] J. D. Chai, D. Stroud, J. Hafner, and G. Kresse, Phys. Rev. B **67**, 104205 (2003).
[10] V. Hugovieux, E. Farhi, M. R. Johnson, F. Juranyi, P. Bourges, and W. Kob, Phys. Rev. B **75**, 104208 (2007).
[11] M. M. G. Alemany, R. C. Longo, L. J. Gallego, D. J. González, L. E. González, M. L. Tiago, and J. R. Chelikowsky, Phys. Rev. B **76**, 214203 (2007).
[12] B. B. Alchagirov and A. M. Chochaeva, High Temp. **38**, 44 (2000); K. H. Schramm, Z. Metallkd. **53**, 316 (1962).
[13] R. B. Gordon, Acta Metall. **7**, 1 (1959).
[14] W. Menz, F. Sauerwald, and K. Fisher, Acta Metall. **14**, 1617 (1966).
[15] Yu. Plevachuk, V. Sklyarchuk, W. Hoyer, and I. Kaban, J. Mater. Sci. **41**, 4632 (2006).
[16] Y. Waseda, *The Structure of Non-Crystalline Materials* (McGraw-Hill, New York, 1980).
[17] D. Jovic and I. Padureanu, J. Phys. C **9**, 1135 (1976).
[18] S. Takeda, S. Tamaki, and Y. Waseda, J. Phys. Soc. Jpn. **53**, 3447 (1984).
[19] T. Itami, S. Munejiri, T. Masaki, H. Aoki, Y. Ishii, T. Kamiyama, Y. Senda, F. Shimojo, and K. Hoshino, Phys. Rev. B **67**, 064201 (2003).
[20] T. Narushima, T. Hattori, T. Kinoshita, A. Hinzmann, and K. Tsuji, Phys. Rev. B **76**, 104204 (2007).
[21] S. Hosokawa, J. Greif, F. Demmel, and C. Pilgrim, Chem. Phys. **292**, 253 (2003).
[22] S. Hosokawa, C. Pilgrim, and F. Demmel, J. Non-Cryst. Solids **353**, 3122 (2007).
[23] N. W. Ashcroft and J. Lekner, Phys. Rev. **145**, 83 (1966); P. Ascarelli, *ibid.* **173**, 271 (1968); J. Phys. F: Met. Phys. **4**, 525 (1974).
[24] W. Jank and J. Hafner, Phys. Rev. B **41**, 1497 (1990).
[25] A. Di Cicco, Phys. Rev. B **53**, 6174 (1996); A. Di Cicco, A. Trapananti, E. Principi, S. Di Panfilis, and A. Filipponi, Appl. Phys. Lett. **89**, 221912 (2006).
[26] V. Petkov and G. Yunchov, J. Phys.: Condens. Matter **6**, 10885 (1994).
[27] S. Baroni, A. Dal Corso, S. de Gironcoli, P. Giannozzi, C. Cavazzoni, G. Ballabio, S. Scandolo, G. Chiarotti, P. Focher, A. Pasquarello, K. Laasonen, A. Trave, R. Car, N. Marzari, and A. Kokalj, http://www.pwscf.org/

[28] D. M. Ceperly and B. J. Alder, Phys. Rev. Lett. **45**, 566 (1980); J. P. Perdew and A. Zunger, Phys. Rev. B **23**, 5048 (1981).
[29] N. Troullier and J. L. Martins, Phys. Rev. B **43**, 1993 (1991).
[30] L. E. González, D. J. González, and M. J. Stott, Phys. Rev. B **77**, 014207 (2008).
[31] X. G. Gong, G. L. Chiarotti, M. Parrinello, and E. Tosatti, Europhys. Lett. **21**, 469 (1993).
[32] J. P. Hansen and I. R. McDonald, *Theory of Simple Liquids* (Academic, London, 2006); J. P. Boon and S. Yip, *Molecular Hydrodynamics* (McGraw-Hill, New York, 1980).
[33] C. Jo and K. Lee, J. Chem. Phys. **113**, 7268 (2000).
[34] U. Balucani and M. Zoppi, *Dynamics of the Liquid State* (Clarendon, Oxford, 1994).
[35] C. H. Ma and R. A. Swallin, J. Chem. Phys. **46**, 3014 (1962).
[36] G. Frohberg, *Material Sciences in Space* (Springer, Berlin, 1986); G. Frohberg, K. H. Kraatz, and H. Weber, in Proceedings of the Sixth European Symposium on Material Sciences under Microgravity Conditions, Bordeaux, 1986.
[37] A. Bruson and M. Gerl, Phys. Rev. B **21**, 5447 (1980).
[38] T. Itami, T. Masaki, H. Aoki, S. Munejiri, M. Uchida, S. Matsumoto, Y. Ishii, K. Kamiyama, and K. Hoshino, J. Non-Cryst. Solids **312–314**, 177 (2002).
[39] L. Sjögren and A. Sjölander, J. Phys. C **12**, 4369 (1979); L. Sjögren, Phys. Rev. A **22**, 2866 (1980).
[40] W. Gudowski, M. Dzugutov, and K. E. Larsson, Phys. Rev. E **47**, 1693 (1993).
[41] K. Hoshino, F. Shimojo, and S. Munejiri, J. Phys. Soc. Jpn. **71**, 119 (2002).
[42] I. M. de Schepper and M. H. Ernst, Physica A **98**, 189 (1979).
[43] W. Moontfrooy, I. de Schepper, J. Bosse, W. Glaser, and Ch. Morkel, Phys. Rev. A **33**, 1405 (1986).
[44] C. Cabrillo, F. J. Bermejo, M. Alvarez, P. Verkerk, A. Maira-Vidal, S. M. Bennington, and D. Martin, Phys. Rev. Lett. **89**, 075508 (2002); J. Phys. Cond. Mat. **16**, S309 (2004).
[45] I. Ebbsjo, T. Kinell, and J. Waller, J. Phys. C **13**, 1865 (1980).
[46] D. J. González, L. E. González, J. M. López, and M. J. Stott, J. Chem. Phys. **115**, 2373 (2001); Phys. Rev. B **65**, 184201 (2002).
[47] A. Torcini, U. Balucani, P. H. K. de Jong, and P. Verkerk, Phys. Rev. E **51**, 3126 (1995).
[48] F. Shimojo, K. Hoshino, and M. Watabe, J. Phys. Soc. Jpn. **63**, 141 (1994).
[49] S. Kambayashi and G. Kahl, Phys. Rev. A **46**, 3255 (1992); G. Kahl and S. Kambayashi, J. Phys.: Condens. Matter **6**, 10897 (1994).
[50] J. Casas, D. J. González, and L. E. González, Phys. Rev. B **60**, 10094 (1999); J. Casas, D. J. González, L. E. González, M. M. G. Alemany, and L. J. Gallego, *ibid.* **62**, 12095 (2000).
[51] N. Yoshimoto, H. Shibata, M. Yoshizawa, K. Suzuki, K. Shigematsu, and S. Kimura, Jpn. J. Appl. Phys., Part 1 **35**, 2754 (1996).
[52] B. Fak and B. Dorner, Institut Laue-Langevin Report No. 92FA008S, 1992.
[53] B. J. Palmer, Phys. Rev. E **49**, 359 (1994).
[54] U. Balucani, J. P. Brodholt, P. Jedlovszky, and R. Vallauri, Phys. Rev. E **62**, 2971 (2000).
[55] M. Shimoji and T. Itami, *Atomic Transport in Liquid Metals* (Trans. Tech. Publications, Aedermannsdorf, Switzerland, 1986).
[56] P. L. Silvestrelli, A. Alavi, M. Parrinello, and D. Frenkel, Phys. Rev. Lett. **77**, 3149 (1996); P. L. Silvestrelli, A. Alavi, and M. Parrinello, Phys. Rev. B **55**, 15515 (1997).
[57] R. Kubo, J. Phys. Soc. Jpn. **12**, 570 (1957); D. A. Greenwood, Proc. Phys. Soc. Jpn. **71**, 585 (1958).
[58] T. Iida and R. I. L. Guthrie, *The Physical Properties of Liquid Metals* (Clarendon, Oxford, 1988).